AIAA Aviation
16-20 June 2014, Atlanta, GA
20th AIAA/CEAS Aeroacoustics Conference

# Auralization of Flyover Noise from Open Rotor Engines Using Model Scale Test Data

Stephen A. Rizzi[1]
*NASA Langley Research Center, Hampton, VA 23681, USA*

*and*

David B. Stephens[2], Jeffrey J. Berton[3], and Dale E. Van Zante[4]
*NASA Glenn Research Center, Cleveland, OH 44135, USA*

*and*

John P. Wojno[5] and Trevor W. Goerig[6]
*GE Aviation, Cincinnati, OH 45215, USA*



**A series of model scale tests were recently completed using the Open Rotor Propulsion Rig at the NASA Glenn Research Center in an effort to characterize the aero/acoustic performance of several open rotor propulsor designs. These included the historical baseline and second generation (Gen-2) blade sets. Subsequently, the Gen-2 design was assessed to have significant cumulative EPNdB margins relative to Chapter 4 noise regulations, whilst the historical blade set had a negative margin. However, integrated metrics like EPNdB are not intuitive to the layperson, and likely do not convey the noise benefits over earlier designs, for example, the acoustically unique UnDucted Fan (UDF®) Demonstrator of the 1980s. This paper develops the means of auralizing flyover noise projections of full-scale open rotor engines using model scale data in a manner that more readily communicates the noise benefit and that is consistent with previously published system noise assessments. The effect of thrust level, installation type, and rotor inflow angle on the generated flyover noise are investigated for the historical baseline blade set. Finally, the benefits of the modern open rotor blade design are made apparent through comparison of flyover noise from the Gen-2 and historical baseline blade sets.**

## Nomenclature

| | | |
|---|---|---|
| $\alpha_{Inflow}$ | = | rotor inflow angle |
| $c_{Flight}$ | = | speed of sound at aircraft flight conditions |
| $c_{Tunnel}$ | = | speed of sound at wind tunnel test conditions |
| $D_{Full\text{-}Scale}$ | = | diameter of rotor for full-scale engine |
| $D_{Rig}$ | = | diameter of rotor for wind tunnel model |
| $f_{Flight}$ | = | frequency of rotor noise at aircraft flight conditions |
| $f_{Static}$ | = | frequency of rotor noise at static conditions |
| $M_{Flight}$ | = | flight Mach number |
| $M_{Tunnel}$ | = | wind tunnel test Mach number |
| $P_{Flight}$ | = | flight static pressure |
| $P_{Tunnel}$ | = | wind tunnel test static pressure |

[1] Senior Researcher for Aeroacoustics, Aeroacoustics Branch, MS 463, Associate Fellow & Lifetime Member AIAA
[2] Research Aerospace Engineer, Acoustics Branch, MS 54-3, Lifetime Member AIAA
[3] Aerospace Engineer, Multidisciplinary Design, Analysis and Optimization Branch, MS 5-11, Senior Member AIAA
[4] Aerospace Engineer, Acoustics Branch, MS 54-3, Senior Member AIAA
[5] Senior Acoustic Engineer, Acoustics and Installation Aerodynamics, 1 Neumann Way, M/D G26
[6] Acoustic Engineer, Acoustics and Installation Aerodynamics, 1 Neumann Way, M/D G26

$\rho_{Flight}$ = air density at aircraft flight conditions
$\rho_{Tunnel}$ = air density at wind tunnel test conditions
$\theta_E$ = noise emission yaw (polar) angle
$\theta_G$ = geometric sideline microphone array angle
*SME* = source motion exponent

## I. Introduction

THE increase in jet fuel costs has prompted renewed research efforts by engine manufacturers in contra-rotating open rotor propulsion systems due to their potential for large reductions in fuel burn relative to contemporary turbofans. Advanced propellers, both single and contra-rotation, were studied in the late 1970s and 1980s for their fuel efficiency benefits as part of the NASA Advanced Turboprop Project.[1] For example, General Electric (GE) had a contra-rotation concept called the UnDucted Fan, UDF®. Multiple generations of early UDF® blade designs were tested at model scale at GE,[2] NASA Lewis,[3] and other locations. Additionally the UDF® demonstrator engine underwent extensive ground tests followed by flight tests on two different commercial aircraft.[4] The UDF® was memorable for its scimitar shaped propeller blades and its unique noise signature.

The UDF® was successful at demonstrating open rotor technology in that it achieved its fuel burn target with acceptable acoustic performance for the regulations at the time. Concept development continued at GE, culminating in the GE36 product design, which was cancelled when changing fuel prices broke down the business model. However, going forward, noise was still a concern and the ability to tailor designs for both high efficiency and low noise was limited by the design tools of that era. The current effort takes advantage of contemporary CFD and CAA tools to optimize blade designs for both aero performance and acoustics. NASA, FAA and GE have collaborated to design, build and test new generations of low-noise, high-efficiency open rotors.[5,6] Aerodynamic performance and acoustics measurements from this test series have been used to perform aircraft system level analyses for fuel burn and acoustics. The new generation of open rotor designs is predicted to have a 15-17 EPNdB cumulative margin relative to Chapter 4 noise regulations for the NASA modern open rotor single aisle aircraft application.[5-7] However, community noise levels based on integrated sound exposure do not adequately capture the remarkable acoustic improvements of the latest generation designs for a layperson. A more natural method of demonstrating the progress in low noise designs would be aural comparisons of a contemporary low-noise propulsor design with the corresponding noise of the original UDF® demonstrator.

Fortunately, a new capability was recently developed to auralize aircraft flyover noise. The process entails synthesis of the source noise, propagation of that noise to a ground receiver, and an optional step of casting that noise in a three-dimensional simulated environment.[8] The approach has been shown to generate pressure time histories having aircraft noise metrics that are consistent with those generated by the NASA Aircraft Noise Prediction Program (ANOPP)[9] system noise prediction tool. The capability was recently demonstrated for a reference state-of-the-art Boeing 777-like aircraft and an advanced Hybrid Wing Body configuration.[10] In that work, source noise definitions used in the synthesis process were obtained from ANOPP semi-empirical models.

Since the source noise prediction models for open rotor engines are a topic of current research,[11] the present effort utilizes the aforementioned wind tunnel test data[5,6] as input for the noise synthesis of both the latest generation Gen-2 concepts, as well as the historical reference blade design. The latter blade was designed for optimal aero performance with no acoustic compromises. The approach taken is similar to that previously used for system noise studies based on this data set, and entails processing the model scale wind tunnel test data to full-scale under flight conditions,[12] with modifications required to separate coherent tonal noise from incoherent broadband noise. The resulting directivity serves as input to the auralization process just as an ANOPP source noise prediction would.

This paper presents the auralization for a straight and level flyover trajectory of a modern open rotor propulsor, designed to power a NASA defined modern narrow-body commercial aircraft concept. In order to illustrate the acoustic improvements of the modern open rotor concepts, the auralized noise spectra focus on the isolated open rotor propulsor without other engine or airframe noise components. The influence of relevant operating conditions and installations are considered for the historical baseline blade set, including the thrust level; installation (isolated versus pylon-mounted); and rotor inflow angle. Finally, the auralized noise generated by the historical baseline is compared to a corresponding auralization of a second generation modern low-noise blade design.

To ensure consistency with the previously published results, community noise metrics derived from the resulting pressure time histories are compared with those generated using the ANOPP Acoustic Data Module with the same underlying data as input. This effort is intended to lay the groundwork for the auralization of flyover noise associated with full aircraft systems incorporating open rotor propulsors to complement system noise predictions of the same.[12]

## II. Open Rotor Acoustic Tests

### A. Test Description

Modern open rotor acoustic testing was conducted at the NASA Glenn Research Center, on the refurbished Open Rotor Propulsion Rig in the acoustically treated 9x15 Low Speed Wind Tunnel, at low speed flight conditions representative of typical aircraft community noise operations. Data were acquired to characterize both off-design aerodynamic performance and acoustics at simulated approach, takeoff, and cutback operating conditions. Isolated and simulated installation model configurations were used. All data used in the present study were acquired at a nominal wind tunnel Mach number of 0.2.

The historical baseline blade set, F31/A31, was the legacy blade set used for the measurements presented here. Recent work[13] demonstrated that the F31/A31 is representative of early 1990s aero design technology noise entitlement. The only compromise for acoustics was associated with the blade count (12 forward x 10 aft). A side view of the blades is shown in Figure 1. Table 1 shows key design parameters. Note that the F31/A31 blade set is different from the earlier 0.72 cruise Mach number design, called F7/A7, which was flown on the UDF® demonstrator aircraft.

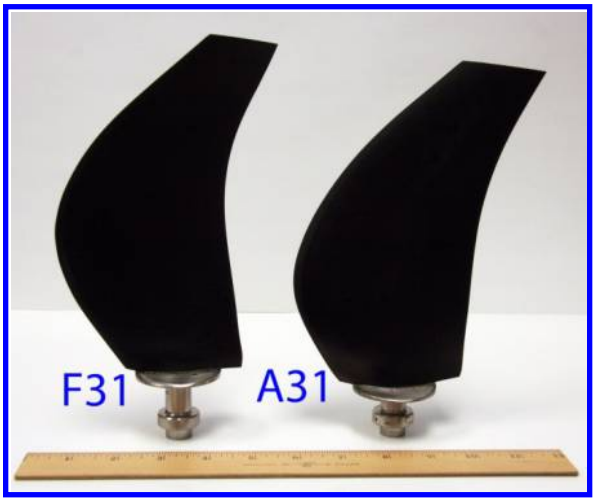


Figure 1: The historical baseline, F31/A31, blade set.

Table 1: Comparison of key parameters for historical and modern designs (full scale).[5]

| *Parameter* | | *Historical* | *Modern* |
|---|---|---|---|
| Blade count | | 12x10 | 12x10 |
| Forward rotor R1 diameter, *D* | m | 3.25 | 4.27 |
| | ft | 10.7 | 14.0 |
| Top of climb disk loading | $kW/m^2$ | 803 | 474 |
| | $hp/ft^2$ | 100 | 59 |
| Spacing/diameter, *S/D* | | 0.28 | 0.27 |
| Design point $PQA/J^3$ | | 0.167 | 0.099 |

Figure 2 and Figure 3 show the F31/A31 blade set in the 9x15 test section in an isolated and a pylon installed pusher configuration, respectively. The primary rotor performance instrumentation were rotating force balances in each rotor hub to measure the thrust and torque of the rotor system. The forward and aft blade rows operated at nominally the same shaft speed. Details of the performance measurements are given by Van Zante et al.[6,14] Acoustic measurements were acquired at a sideline distance of 152.4 cm (60 in) at 18 stops with the traversing microphone shown in Figure 2. The nominal geometric angles associated with each stop were measured relative to zero on-axis upstream with 90º at the aft pitch change axis, and ranged from 140º (stop 1 - downstream) to 17.6º (stop 18 - upstream), see Table 2. Emission angles are discussed in the next section. The microphone signal was digitized at 200 kHz for 15 seconds per directivity angle. Spectra were generated using a $2^{14}$-point FFT resulting in a frequency bin width of 12.2 Hz. Tests were also conducted to estimate the facility's tare background noise levels with no power supplied to the open rotor test article and with no blades attached. Details of the acoustic processing, instrument corrections, atmospheric corrections, etc. are provided by Elliott.[15]

Table 2: List of nominal geometric and emission angles for Mach 0.2.

| Stop Number | 1 | 2 | 3 | 4 | 5 | 6 | 7 | 8 | 9 |
|---|---|---|---|---|---|---|---|---|---|
| | 10 | 11 | 12 | 13 | 14 | 15 | 16 | 17 | 18 |
| Geometric Angle (deg) | 140.0 | 135.0 | 127.5 | 120.0 | 112.5 | 105.0 | 97.5 | 90.0 | 82.5 |
| | 75.0 | 67.5 | 60.0 | 52.5 | 45.0 | 37.5 | 30.0 | 22.5 | 17.6 |
| Emission Angle (deg) | 132.6 | 126.9 | 118.3 | 110.0 | 101.9 | 93.9 | 86.1 | 78.5 | 71.0 |
| | 63.9 | 56.8 | 50.1 | 43.4 | 36.9 | 30.5 | 24.3 | 18.1 | 14.2 |

Figure 2: Isolated open rotor test configuration in the 9x15 LSWT test section showing the acoustic traverse microphone at the 152.4 cm (60 inch) sideline position.

Figure 3: Close-up photo of the open rotor test configuration in the 9x15 LSWT test section with the pylon installed ahead of the rotor system.



**B. Data Processing**

The model scale wind tunnel data was post-processed for use in ANOPP noise assessments and for auralization. The procedure differs slightly depending on the particular usage.

*1. Tunnel to Flight Condition Processing*

The process developed by Guynn et al[12] for converting scale model wind tunnel acoustic data to full-scale flight condition data was adopted with minor changes for auralization. The process is summarized here. Calibrated microphone-corrected Power Spectral Densities (PSDs) (dB/Hz) were adjusted to a 1-ft. free-field, lossless condition through application of an inverse atmospheric attenuation model and spherical spreading loss correction. At each stop, the PSDs of the tare and test data were first converted to narrowband wind tunnel sound pressure levels according to

$$SPL = PSD + 10\log_{10}(\Delta f) \tag{1}$$

where $\Delta f$ is 12.2 Hz.

The tare data was next removed from the test data to obtain the corrected tunnel measurement, that is,

$$SPL_{Tunnel} = 10\log_{10}\left[10^{\left(SPL_{test}/10\right)} - 10^{\left(SPL_{tare}/10\right)}\right]. \tag{2}$$

Low frequency noise below 700 Hz (model scale) was removed from the resultant by replacing that data with a quadratic function having a 10 dB down point (relative to the level at 700 Hz) at 100 Hz.

The data were next converted from wind tunnel to static conditions by

$$\begin{aligned} SPL_{Static} &= SPL_{Tunnel} + 10\log_{10}[1 - M_{Tunnel}\cos\theta_E]^{SME} - 10\log_{10}[(\rho_{Tunnel}/\rho_{ISA})^2 (c_{Tunnel}/c_{ISA})^4] \\ &= SPL_{Tunnel} + 10\log_{10}[1 - M_{Tunnel}\cos\theta_E]^{SME} - 10\log_{10}(P_{Tunnel}/P_{ISA})^2 \end{aligned} \tag{3}$$

where the second term on the right hand side removes the effect of convective amplification included in the measured tunnel data, and the third term is a source strength amplitude adjustment to correct the tunnel conditions to International Standard Atmosphere (ISA) conditions. Here, $M_{Tunnel}$ and $P_{Tunnel}$ are the Mach number and static pressure averaged over all stops, the source motion exponent ($SME$) is taken as 2 for a dipole source, and the emission angle $\theta_E$ is computed from the geometric angle $\theta_G$ by

$$\theta_E = \theta_G - \sin^{-1}[M_{Tunnel}\sin\theta_G]. \tag{4}$$

A list of emission angles is also provided in Table 2 for the nominal $M_{Tunnel}$ of 0.2. Note that there is no associated Doppler frequency shift since the relative velocity between the source and the microphone is zero.

The data were next converted from static conditions to flight conditions by

$$SPL_{Flight} = SPL_{Static} - 10\log_{10}[1 - M_{Flight}\cos\theta_E]^{SME} + 10\log_{10}[(\rho_{Flight} / \rho_{ISA})^2 (c_{Flight} / c_{ISA})^4] + 10\log_{10}[M_{Flight} / M_{Tunnel}]$$
$$= SPL_{Static} - 10\log_{10}[1 - M_{Flight}\cos\theta_E]^{SME} + 10\log_{10}(P_{Flight} / P_{ISA})^2 + 10\log_{10}[M_{Flight} / M_{Tunnel}] \quad (5)$$

where the second term on the right hand side adds the effect of convective amplification for the particular $M_{Flight}$, and the third term adjusts the source strength amplitude to correct the static condition to flight conditions for a standard acoustic day (ISA + 18ºF). The fourth term on the right hand side is an additional correction to account for observed increases in source level with free stream Mach number.

When the data is to be used as input to the ANOPP Acoustic Data Module, the Doppler frequency shift

$$f_{Flight} = f_{Static} / [1 - M_{Flight}\cos\theta_E] \quad (6)$$

must be applied. However, this factor is not applied when the data is used as input to auralization because the propagation process simulates the Doppler shift (see Section III).

Conversion from model scale to full-scale affects both amplitudes and frequencies. The amplitudes were adjusted by the area scale factor

$$SPL_{Flight@Full-Scale} = SPL_{Flight} + 20\log_{10}[D_{Full-Scale} / D_{Rig}] \quad (7)$$

and the frequencies were adjusted by the linear scale factor

$$f_{Flight@Full-Scale} = f_{Flight} / [D_{Full-Scale} / D_{Rig}]. \quad (8)$$

*2. ANOPP-Specific Processing*

The full-scale flight condition narrowband spectra obtained from Eq. (7) are interpolated at emission angles ranging from 10º to 170º in 1º increments. Processed data from stops 1 and 18 are used at emission angles aft of stop 1 and forward of stop 18, respectively. That is, the data are not extrapolated beyond the range of measurements. Next, the frequency vector at each angle increment is Doppler shifted and adjusted to full-scale using Eqs. (6) and (8). In this manner, the data continues to be Doppler shifted outside of the range of measurements even though the underlying source spectra remain unchanged. Finally, data from each angle increment are summed into 1/3-octave bands ranging from 50 Hz to 10 kHz.[16] The resulting data serve as input to the ANOPP Acoustic Data Module,[12] which does not apply any further convective amplification correction or Doppler shift. Noise metrics are computed at 0.5s receiver time intervals after the 1/3-octave band data are propagated though a specified atmosphere to ground receiver(s).

*3. Auralization-Specific Processing*

Since most steps of the auralization process are well understood (see Section III), the main challenge in the auralization of open rotor noise is the development of a source noise synthesis method using data that is both harmonically rich and broadband in nature. It will be shown in Section IV that a synthesis approach which treats the entire broadband spectra as incoherent noise results in a sound that does not compare well with the sound on which it is based, even though the two power spectra may be the same. Thus, the crux of the open rotor auralization is the development of a synthesis approach which treats tones as coherent noise and the remaining broadband spectra as incoherent noise.

The separation of tonal and broadband components is accomplished through application of a 10-point moving median filter. The filter is applied to the full-scale flight condition spectra obtained from Eq. (7) and spectral lines exceeding the median value are replaced by the median value to obtain the broadband component spectra.[17] This is analogous to mowing the lawn with a blade height adjustment made through padding the median value. In this study, padding is used to raise the median value by 1 dB. The resulting broadband component is subtracted from the original full-scale flight condition spectra to obtain the tonal component spectra. Up to 200 tonal amplitudes are obtained by summing seven spectral amplitudes, that is, at the shaft order (SO) frequencies plus three spectral lines on either side, to account for the fact that the tonal peak may be spread over multiple spectral lines. The SO frequencies are obtained using the average of the forward and aft blade shaft speeds, averaged over all stops. This ensures that the synthesized tones do not vary due to small changes in shaft speed between blade rows or emission angles. The broadband spectral amplitudes are set to zero above the maximum non-Doppler shifted frequency of the 10 kHz 1/3-octave band (approximately 14.8 kHz) to eliminate very high frequency tunnel noise associated with the forward-most emission angles. The broadband and tonal noise are synthesized as separate components, similar to the manner in which fan noise was synthesized in the prior study,[10] then added to obtain the total open rotor noise.

As in the ANOPP processing, the source spectra are interpolated and use the last available data outside the measured range. However, this interpolation is performed during the synthesis operation. Finally, it is important to note that the frequency vector for the auralization is full-scale adjusted per Eq. (8), but not Doppler-shifted per Eq. (6). Doppler shift is simulated in the propagation process, as described in Section III.B.

## III. Auralization Methodology

Like the system noise prediction, the auralization methodology takes a source-path-receiver approach. Pressure time histories of the source are synthesized from broadband and tonal amplitude source noise hemispheres obtained from the post-processed test data. Propagation of the pressure time histories to a ground receiver is performed in the time domain based on the path, and simulates spherical spreading loss, atmospheric absorption, Doppler shift via time-varying propagation time delay, and ground plane reflection. The received pressure time history for the flyover may be post-processed to obtain integrated metrics, or auralized with or without an additional step of three-dimensional (3D) audio simulation.

### A. Source Noise Synthesis

The pressure time history at the source position is synthesized at emission time based upon the instantaneous source spectrum. The instantaneous source spectrum is, in general, a function of both the emission angle and the operational state of the aircraft. In the present study, the operational state does not vary over the course of the flyover. The emission angle is determined by the straight-line path between the source and receiver and is typically calculated at an update rate on the order of 100 Hz. The operational state is specified at waypoints in the trajectory at a much lower rate on the order of seconds. Note that because convective amplification is incorporated in the source noise hemispheres, its effect is automatically realized in the synthesized signal. This synthesis approach has been implemented in the NASA Aircraft Source Noise Generator (ASoNG) synthesis program[8,18-20] and is depicted in Figure 4.

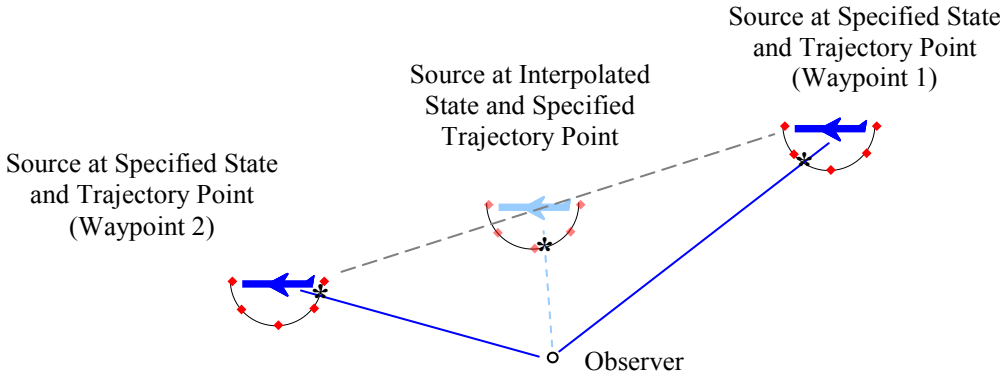


Figure 4: Synthesis is performed at the directivity angle (denoted by *) at the time of emission.

The ASoNG program synthesizes pressure time histories in a manner dependent on the source spectrum specified. A pressure time history that continually evolves with changes in source directivity is critical in order to avoid sudden changes in character resulting from a discretized source spectrum. For spectra expressed in PSD form, ASoNG synthesizes the broadband noise using an overlap-add technique.[8,18] For spectra expressed as tonal amplitudes, ASoNG synthesizes the noise in the time domain in a manner which permits changes in amplitude and frequency as a function of time.[20] The output of the synthesis process is analogous to the signal a microphone would record at some reference distance near the flying source. As the source moves, the emission angle changes in a continuous fashion and, by analogy, the microphone location smoothly traverses the hemisphere below the aircraft. In this manner, the source directivity is embedded in the synthesized signal and does not need to be explicitly represented in the propagation stage. This approach to synthesis makes simulation of arbitrary trajectories straightforward.

#### *1. Broadband Synthesis*

Broadband synthesis employed herein is a derivative of that developed for source spectra specified in 1/3-octave bands, and is based on a subtractive synthesis operation using an overlap-add procedure.[8,18] For each processing block, the instantaneous narrowband source spectrum is obtained via interpolation and each narrowband frequency component is assigned a random phase. The resulting complex function is inversely transformed to obtain the

pressure time history. The next processing block corresponds to a point later in the trajectory. It is not contiguous, but overlaps the preceding block. Its processed output time history is added to that of the previous block at a time offset (hop size) corresponding to the amount of overlap. In this manner, the synthesized signal smoothly transitions with changes in source directivity. Note that the broadband synthesis is performed at the sampling rate associated with the processed data, then resampled post-synthesis to the audio sampling rate of 44.1 kHz. This avoids interpolation of the spectra in the frequency domain, which can be error prone.

*2. Synthesis of Tones*

Synthesis of tones is performed in the time domain using an additive technique. Each tone, in general, may be represented as an amplitude and frequency-modulated cosine wave, as in

$$s_k(t) = a_k(t)\cos\left(\phi_k(t)\right) \tag{9}$$

where $a_k(t)$ is the amplitude envelope of the $k^{th}$ tone and $\phi_k(t)$ is the phase argument of the $k^{th}$ tone in radians. According to Eq. (9), each harmonic is characterized completely by two parameters; the amplitude and phase functions. The relationship of the time-varying frequency of the cosine term to the phase argument in the single-tone model is described by

$$\phi_k(t) = 2\pi\int_{-\infty}^{t} f_k(\tau)\,d\tau + \phi_{o,k} \tag{10}$$

where $f_k$ is the instantaneous frequency of the $k^{th}$ tone in Hz, $\tau$ is a dummy variable of integration and $\phi_{o,k}$ is the initial phase. This expression for the phase allows for variations in frequency due to changes in operating condition or unsteadiness of the source, as described below. Note that a tone of constant (time-invariant) frequency $f$ will have a phase integral that becomes the familiar $2\pi ft$ argument of a simple harmonic oscillator. The instantaneous frequency may be obtained from Eq. (10) by differentiating with respect to time as

$$f_k(t) = \frac{1}{2\pi}\frac{d\left(\phi_k(t)\right)}{dt} \tag{11}$$

The tonal amplitudes are varied continuously according to the instantaneous emission angle of the source noise hemisphere. The initial phase of each harmonic is randomized. Pressure time histories are synthesized for contiguous blocks of specified hop size. A continuous waveform is achieved by maintaining phase between subsequent blocks. Changes in the tonal frequencies do not occur within a single hemisphere corresponding to one operating condition, but may occur between different operating conditions, e.g. an engine spool up. All tones are summed to obtain the total tonal noise. Note that while the tonal synthesis can be performed at any sampling rate irrespective of the tonal frequencies, the sampling rate used for the broadband synthesis was used for consistency, necessitating post-synthesis resampling to the audio sampling rate of 44.1 kHz.

*3. Temporal Variations*

The source noise hemispheres are generated from time-averaged test data and are therefore time invariant. Broadband and tonal syntheses based on these models faithfully reproduce the predicted spectra when averaged over time, but lack the temporal variations found in the test data. The absence of temporal variations is observable and may diminish fidelity,[21] which in this context refers to the accuracy of the synthesized sound when compared to the wind tunnel recording.

Analyses of jet noise[22] and tonal fan noise[20] data obtained from static engine tests have previously been performed to characterize the fluctuations, and these fluctuations were subsequently introduced into the source noise synthesis. While no such analysis has been performed on the open rotor test data, it is possible that a similar approach could be taken. However, this is outside of the scope of the present effort.

## B. Propagation

Propagation of the source noise to a ground receiver occurs in the time domain through application of a time-dependent gain, time delay, and filter to the source noise.[8,18] The propagation process accounts for spherical spreading loss, atmospheric absorption and time delay, as well as optionally including ground plane reflection. The time varying nature of these quantities is governed by the propagation path.

The straight-line path between the source and receiver is computed at evenly spaced emission times corresponding to the synthesis hop size. Spherical spreading loss is dependent on the slant range, giving a time-dependent negative gain. The time delay is a function of the speed of sound and slant range, and its time rate of change simulates Doppler shift. Note that this scheme applies at all emission angles, including those ahead of the forward-most stop and aft of the aft-most stop, even though the synthesized source noise does not use extrapolated

spectra. Because the time delay is not generally an integer multiple of the audio sampling rate, fractional delay processing[23] is required to avoid audible artifacts in the propagated sound. As previously noted, the only accurate and consistent approach between ANOPP and the auralization is to specify a uniform atmosphere to ensure a constant speed of sound along the straight-line propagation path.[10]

Atmospheric absorption is accumulated along the straight-line path through the specified atmosphere at each 1/3-octave band center frequency. The absorption curve is fit with a $2^n$-point spline and converted to a minimum phase finite impulse response (FIR) filter via an inverse fast Fourier transform (FFT), as described by Rizzi et al.[18] The filter is slant range dependent and therefore varies in time with the moving source.

Once the time-dependent gain, time delay, and filter are known, the synthesized signal is propagated by filtering the time-delayed signal in the time domain and applying the time-dependent spreading loss to the result. The propagation stage is performed on a dedicated audio server[24] as part of the NASA Community Noise Test Environment[8] (CNoTE) simulator application. The output of the propagation stage is a pseudo-recording at the receiver location.

Finally, ground plane reflection may be optionally applied according to either a hard surface (infinite) or finite impedance boundary.[25,26] In this study, a hard (infinite impedance) boundary is considered. The effect of ground plane reflection is simulated with an image source. The reflected path is processed in a similar manner to that described above for the direct path, but with a time-varying delay line, gain, and atmospheric absorption filter associated with the image ray. The interference caused by the addition of the propagated direct and reflected rays produces a comb filter effect,[27] which alters the spectral content in a time-varying manner as the aircraft moves along its trajectory.

Pseudo-recordings of the propagated synthesized noise are post-processed using the ANOPP2[28] Acoustic Analysis API to generate A-weighted Sound Pressure Level (SPL) in dB (re: 20 μPa), Tone Corrected Perceived Noise Level (PNLT) in PNdB, and Effective Perceived Noise Level (EPNL) in EPNdB for comparison with ANOPP generated metrics. This is possible because engineering units are maintained through the auralization process.

## IV. Results

The noise generated under various operating conditions and installations is next considered for the historical baseline and second generation blade sets. In particular, the effect of thrust level, installation type (pylon-mounted or isolated), rotor inflow angle, and blade set are investigated. These are first performed for a receiver flush to a hard ground plane to allow the trends to be more easily seen in the SPL and PNLT traces. Two cases are examined for a receiver above the ground to assess the effect of reflections on the received noise. The range of test conditions considered is presented in Table 3. Subsequent plots and discussion refer to the reading number as shorthand notation for each condition.

Table 3: Open rotor test conditions investigated.

| Reading Number | Blade Set | Installation | Full-Scale Thrust (lbf) | $\alpha_{Inflow}$ (deg) | Forward BPF (Hz) | Aft BPF (Hz) |
|---|---|---|---|---|---|---|
| 359 | F31/A31 | Pylon | 13741 | 0 | 258 | 215 |
| 361 | F31/A31 | Pylon | 14650 | 0 | 264 | 220 |
| 470 | F31/A31 | Isolated | 13609 | 0 | 260 | 217 |
| 480 | F31/A31 | Isolated | 13566 | 3 | 260 | 217 |
| 488 | F31/A31 | Isolated | 13686 | 8 | 260 | 217 |
| Gen-2* | Gen-2 | Pylon with mitigation | 14472 | 0 | n/a | n/a |

* GE Proprietary Data (not available for download)

For simplicity, flyover noise is simulated for a steady, overhead, and level flight trajectory at Mach 0.25 at an altitude of 500 ft. above field elevation. The total length of the flyover is 40k ft. and extends 20k ft. on either side of the receiver. A twin-rotor flight vehicle is considered, adding $10\log_{10}(2)$ to the open rotor source noise. No other sources, e.g. engine core, jet or airframe noise, are considered. A homogeneous atmosphere for a standard acoustic day (ISA + 18ºF) is used and atmospheric absorption is obtained using the ANSI model with the Zuckerwar update.[9] The ground is considered acoustically hard and the receiver is either flush to the ground, resulting in a 6.02 dB increase across all frequencies, or at the certification microphone height of 3.937 ft. (120 cm). Because of the low frequency tonal content, the tone correction penalty for PNLT calculations considers all tones in the 50 Hz – 10 kHz 1/3-octave band range, i.e. it does not disregard tones under 800 Hz 1/3-octave band as is sometimes done in

turbofan applications. In the following, selected supplemental audio clips are available for download via the Internet.[29]

### A. Synthesis Validation

In order to validate the source noise synthesis process, as-measured, calibrated, but otherwise uncorrected, microphone pressure time history data from reading 361 at stop 1 ($\theta_E$ = 132.6º) were used. This allowed the synthesized sound to be both qualitatively (aurally) and quantitatively compared with the recording. The PSD was generated from high pass filtered versions of the data with a cutoff frequency of 550 Hz. The process described for separating tonal and broadband components was applied and the resulting data served as input to the component synthesis. In addition, synthesis of the unseparated PSD was performed to demonstrate the need for treating tones as a coherent noise source.

Shown in Figure 5 is a comparison of the PSD derived from the synthesized tonal signal with that of the separated measured data for the first 50 shaft orders. Here both the PSD of the synthesized tonal pressure time history and separated measurement were summed at the SO frequencies plus three spectral lines on either side. Excellent agreement is also noted in the comparison of the PSD derived from the synthesized broadband spectrum and the separated broadband measured data, as seen in Figure 6.

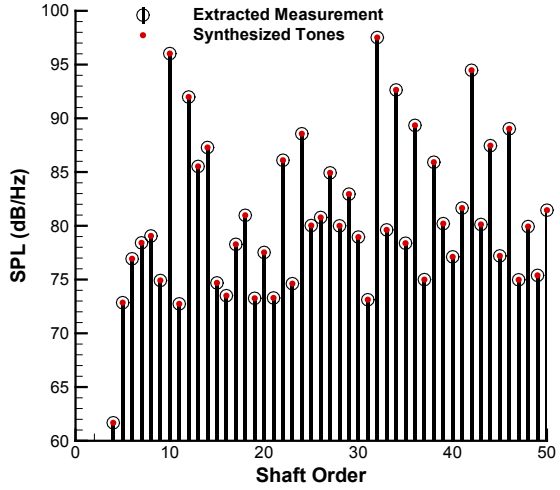


Figure 5: PSD of synthesized and measured (separated) tonal data for reading 361 (model scale).

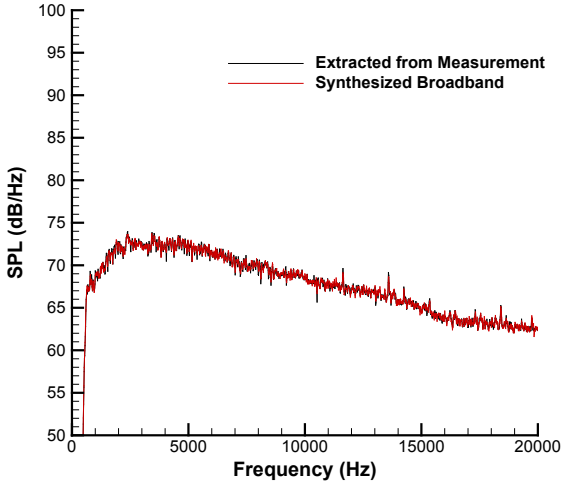


Figure 6: PSD of synthesized and measured (separated) broadband data for reading 361 (model scale).

The sum of synthesized tonal and broadband components constitutes the total source noise at this directivity angle and the comparison of its PSD with that of the measurement in seen in Figure 7. The two PSDs compare very well. The PSD of the synthesized noise obtained from only broadband synthesis of the total, unseparated measured PSD also compares very well, but is not shown for clarity. For that synthesis method, the entire spectrum is treated as incoherent broadband noise. While both synthesized spectra compare favorably with the measured PSD, the auralized sounds differ. In particular, the sum of separately synthesized broadband and tonal noise (supplemental audio.S1) is nearly indistinguishable from the measured data (supplemental audio.S2), whilst the broadband-only synthesis exhibits an undesirable warble-like artifact (supplemental audio.S3). The data provided here demonstrate the effectiveness of the method for separating components for synthesis.

### B. Effect of Thrust

The effect of thrust on open rotor flyover noise is considered through comparison of two pylon-mounted, zero inflow angle conditions; reading 359 with a full-scale thrust of 13,741 lbf. and reading 361 with a 6.6% higher full-scale thrust of 14,650 lbf. The A-weighted SPLs for both flyovers are shown in Figure 8, where it is seen that the higher thrust level associated with reading 361 has a small effect at the forward emission angles and a greater effect at the aft emission angles. The excellent agreement between the auralization and ANOPP analyses demonstrates the compatibility of the two approaches. In Figure 8 and subsequent similar plots, the emission angle at the receiver time is shown below. The dashed horizontal lines delimit the range of emission angles. Here it is seen that the second of two peaks in each trace are coincident with the last emission angle, occurring at about 72.8s receiver time. The decrease from that point on is solely attributable to spreading loss and atmospheric attenuation. This highlights

a known limitation of this data set, that is, the aft-most measurement angle may not be sufficiently aft to fully characterize the source directivity.

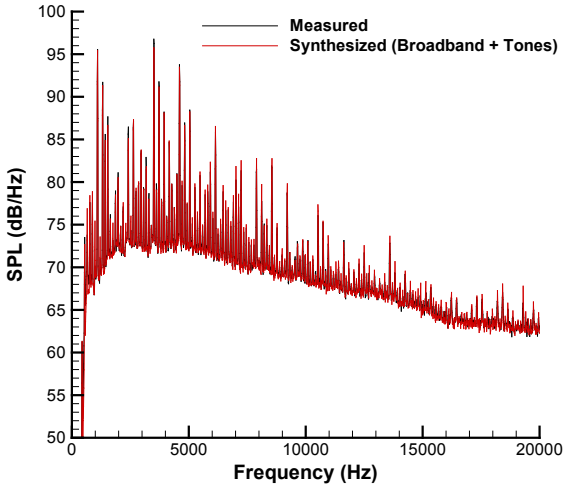


Figure 7: PSD of synthesized and measured total noise for reading 361 (model scale).

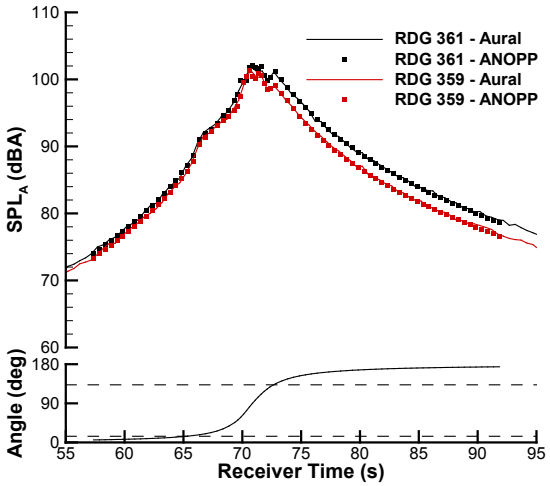


Figure 8: A-weighted SPL for two flyovers with different thrust levels (flush receiver).

Next we consider the PNLT traces shown in Figure 9. Here good agreement is shown between the two traces, with small differences attributable to the different methods of propagation; 1/3-octave band in the case of ANOPP and time domain in the case of the auralization. Also shown are the horizontal lines indicating levels 10 PNdB down from the maximum PNLT. EPNL is calculated using data above these lines. In both cases, a significant portion of the integrated area above each line is aft of the last available emission angle. Notwithstanding this, the calculated metrics compare very well (see Table 4). To gain some insight into the higher noise levels associated with the higher thrust, it is useful to look at a breakdown of A-weighted SPL and PNLT between tonal and broadband components, as shown in Figure 10. It is seen that the tonal and broadband contributions are comparable on the approach side, while the retreating side is dominated by the tonal contribution. Also noteworthy is the observation that the peak of the broadband noise PNLT occurs near the 90º emission angle and is about 2 EPNdB down from the peak of the tonal noise PNLT, which occurs at the aft-most emission angle. Finally, this type of information is readily available from the auralization process because the two components are synthesized and propagated separately. While such analyses could as well be performed in ANOPP with separated 1/3-octave band source spectra, it is not expedient to do so.

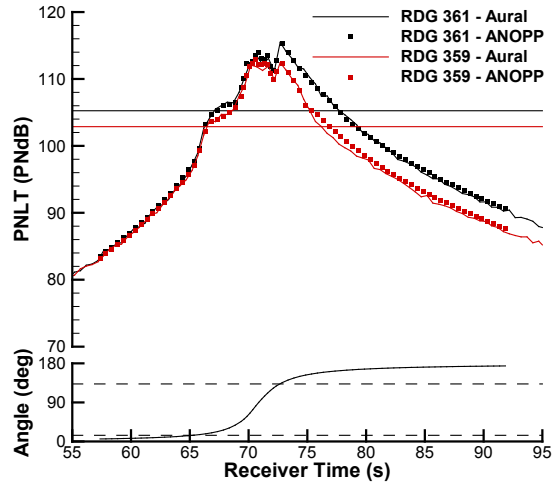


Figure 9: PNLT for two flyovers with different thrust levels (flush receiver).

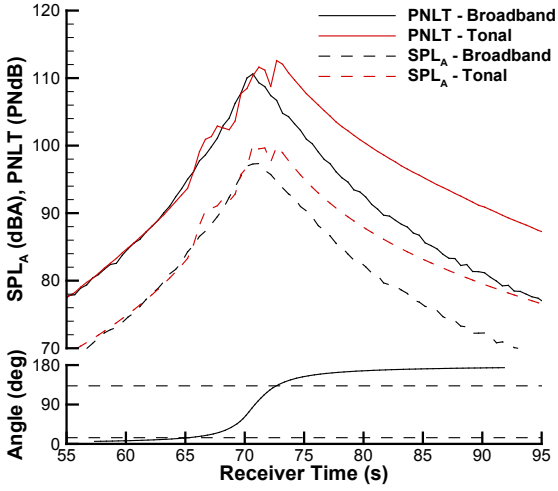


Figure 10: Breakdown of tonal and broadband metrics from auralization for reading 361 (flush receiver).

Table 4: Effect of thrust on EPNL.

| Reading Number | Full-Scale Thrust (lbf) | ANOPP (EPNdB) | Auralization (EPNdB) |
|---|---|---|---|
| 359 | 13741 | 109.3 | 109.0 |
| 361 | 14650 | 111.3 | 111.3 |

The noise metrics in Figure 10 are useful for indicating that the significant effect of thrust on the retreating side is tone related. To further elucidate this effect, we turn our attention to the non-Doppler-shifted, full-scale spectral plots in Figure 11 and Figure 12 for the aft and forward emission angles, respectively. At the aft emission angle, a greater than 3 dB rise in SPL from the lower thrust level to the higher thrust level is shown for the 1F+2A combination tone (SO 32 at 689 & 703 Hz). Other tones are comparable in level. A more detailed analysis is required to better understand this phenomenon, but such an undertaking is outside the scope of this paper. At the forward emission angle, it is seen that all tonal amplitudes are comparable between the two thrust levels, see Figure 12.

Auralizations of flyover noise associated with readings 359 and 361 are provided as supplemental audio.S4 and audio.S5, respectively. The reading 361 flyover noise is noticeably louder. An interleaved version which cuts back and forth between the two readings is provided in supplemental audio.S6.

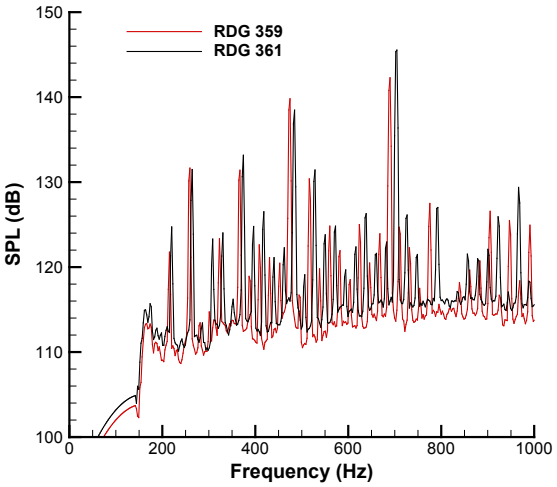


Figure 11: Effect of thrust on full-scale source spectra at the aft emission angle.

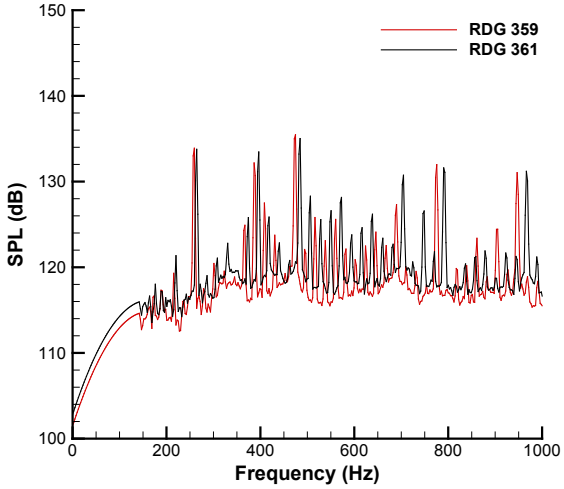


Figure 12: Effect of thrust on full-scale source spectra at the forward emission angle.

### C. Effect of Propulsor Installation

The effect of propulsor installation on open rotor flyover noise is considered through comparison of two conditions having comparable thrust (<1% variance) and zero inflow angle conditions; reading 359 in a pylon-mounted condition and reading 470 in an isolated condition. The presence of the pylon has negligible effect on the approach side A-weighted SPL, with significant differences noted only in the last emission angle on the retreating side, see Figure 13. Similar behavior is noted in the PNLT traces shown in Figure 14. The ANOPP and auralization traces are consistent, with small differences only seen in the PNLT traces. A penalty of about 1 EPNdB is incurred in the pylon-mounted configuration, as indicated in Table 5.

On the retreating side, the 1F+1A combination tones (SO 22 at 476 Hz) are comparable for both installations, as seen in Figure 15. However, the 1F+2A combination tone (SO 32 at 689 Hz) for the pylon-mounted configuration is almost 4 dB higher than the isolated condition. Harmonics of the forward and aft BPF tones are also stronger for the pylon-mounted case, notably at 1A (SO 10 at 215 Hz), 1F (SO 12 at 258 Hz) and 2F (SO 24 at 516 Hz), as are most other SO tones. This is consistent with the once per revolution change in loading as the blades pass through the velocity deficit aft of the pylon. On the approach side, the isolated installation has virtually no 1F BPF tone (SO 12 at 260 Hz) or 3F BPF tone (SO 36 at 780 Hz), while those tones are strong in the pylon-mounted case, see Figure 16. Conversely, the 1F+1A combination tone (SO 22 at 476 Hz) for the isolated case is almost 3 dB higher than the same tone for the pylon-mounted case. A more detailed analysis of the noise generation mechanisms is outside the scope of this study.

Due to its generally stronger tonal amplitudes, the auralized flyover of the pylon-mounted case sounds both louder and harsher than the isolated case (supplemental audio.S7). An interleaved version is available as supplemental audio.S8.

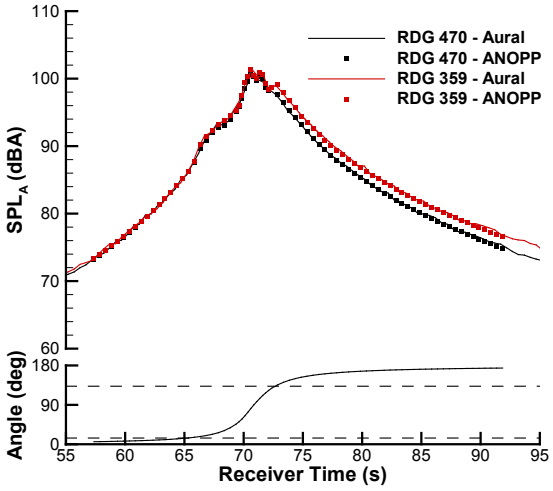


Figure 13: A-weighted SPL for two flyovers with different propulsor installations (flush receiver).

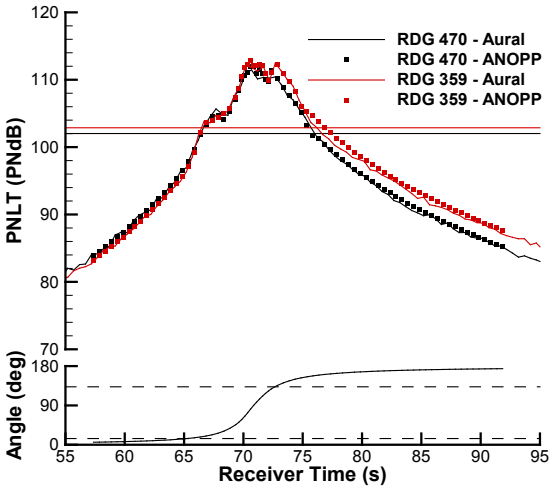


Figure 14: PNLT for two flyovers with different propulsor installations (flush receiver).

Table 5: Effect of propulsor installation on EPNL.

| Reading Number | Installation | ANOPP (EPNdB) | Auralization (EPNdB) |
|---|---|---|---|
| 359 | Pylon | 109.3 | 109.0 |
| 470 | Isolated | 108.1 | 108.0 |

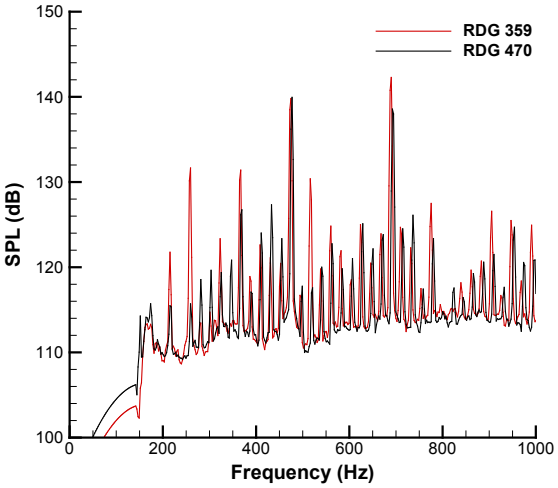


Figure 15: Effect of propulsor installation on full-scale source spectra at the aft emission angle.

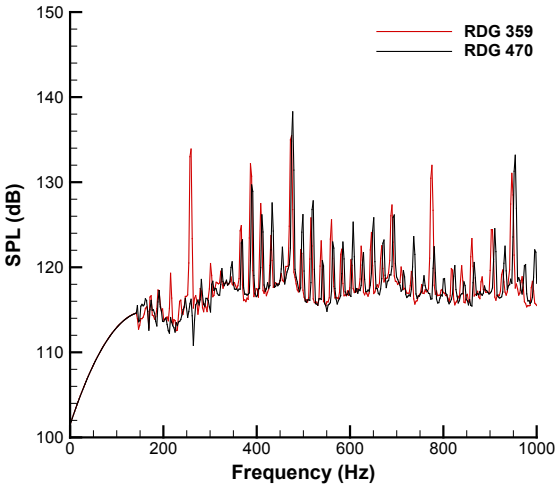


Figure 16: Effect of propulsor installation on full-scale source spectra at the forward emission angle.

### D. Effect of Rotor Inflow Angle

The effect of rotor inflow angle is considered through comparison of three isolated mounting conditions having comparable thrust (<1% variance); readings 470, 480, and 488 with $\alpha_{Inflow}$ = 0º, 3º, and 8º, respectively. The rotor inflow angle is seen to have a significant effect on the A-weighted SPL and PNLT, as shown in Figure 17 and Figure 18, respectively. Further, unlike the previous cases considered, differences are seen on both the approach side and retreating side. Significant differences on the approach side are attributable to the forward emission angle data (stop 18), which extends from the start of the run until roughly 67.4s, where the stop 17 data is used. This

behavior has little bearing on EPNL however, as the data used in that calculation intersect the 10 PNdB down line near the transition point. There is only about a 0.5 EPNdB penalty associated with the 3º inflow angle data, but roughly 1.5 EPNdB additional penalty associated with the 8º inflow angle data, see Table 6.

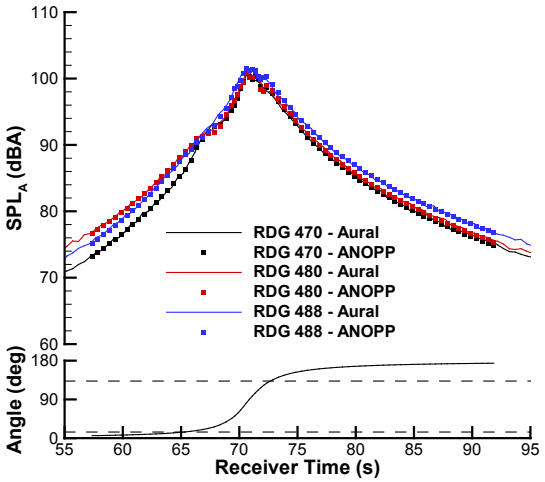


Figure 17: A-weighted SPL for three flyovers with different rotor inflow angles (flush receiver).

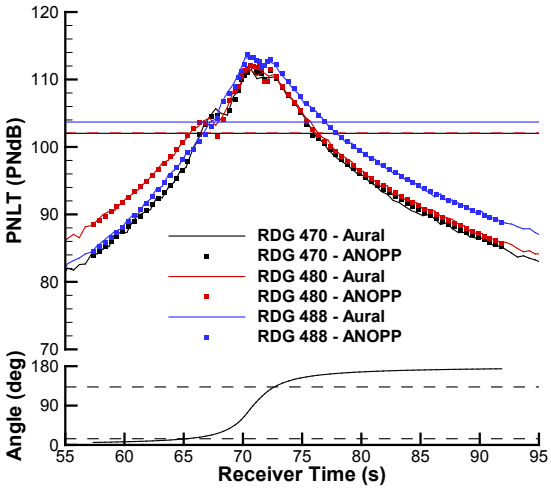


Figure 18: PNLT for three flyovers with different rotor inflow angles (flush receiver).

Full-scale source spectra for forward and aft emission angles are next considered to help explain the flyover metrics. The forward emission angle spectra are shown in Figure 19 and Figure 20, and the aft emission angle spectra are shown in Figure 21 and Figure 22. Two figures are presented for each angle to provide clarity amongst the different rotor inflow angles. The first observation is that the forward angle is dominated by combination tones 1F+1A (SO 22 at 476 Hz), 1F+2A (SO 32 at 694 Hz), and 2F+2A (SO 44 at 954 Hz). While these tones are also significant at the aft angle, the relative contribution of other tones increases.

Table 6: Effect of rotor inflow angle on EPNL.

| Reading Number | $\alpha_{Inflow}$ (deg) | ANOPP (EPNdB) | Auralization (EPNdB) |
|---|---|---|---|
| 470 | 0 | 108.1 | 108.0 |
| 480 | 3 | 108.6 | 108.4 |
| 488 | 8 | 110.0 | 110.0 |

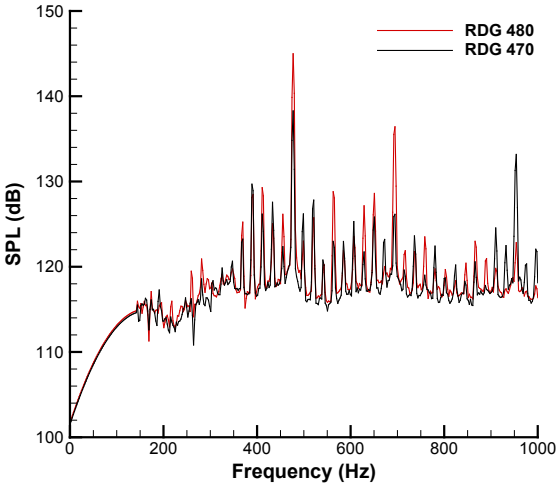


Figure 19: Full-scale source spectra for rotor inflow angles of 0º and 3º at the forward emission angle.

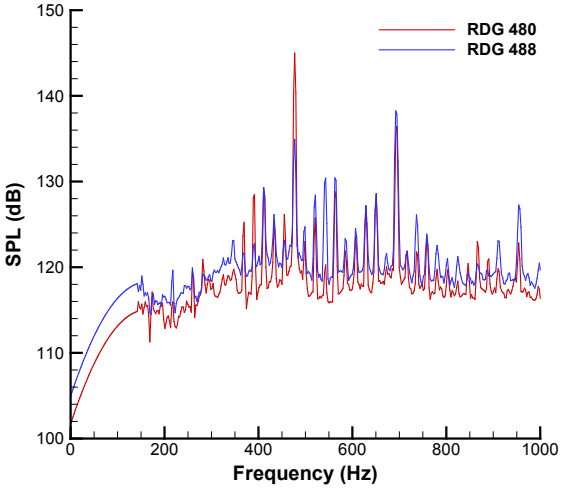


Figure 20: Full-scale source spectra for rotor inflow angles of 3º and 8º at the forward emission angle.

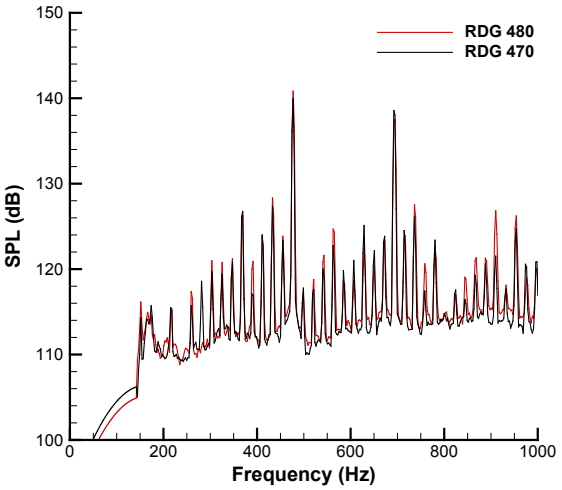


Figure 21: Full-scale source spectra for rotor inflow angles of 0º and 3º at the aft emission angle.

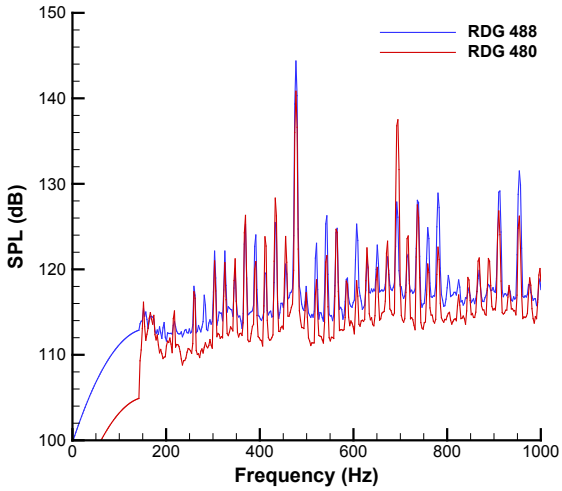


Figure 22: Full-scale source spectra for rotor inflow angles of 3º and 8º at the aft emission angle.

Focusing now on the forward angle, for the dominant 1F+1A tone, there is an increase of 6.7 dB as $\alpha_{Inflow}$ progresses from 0º (reading 470) to 3º (reading 480), but then a decrease of 10 dB progressing to 8º (reading 488). Previous research has shown that the rotor inflow angle has a strong influence on the trajectory of the front rotor tip vortex.[30] The interaction of this vortex with the aft blades is strongly linked to the 1F+1A tone,[5] and this effect appears to be accentuated for the 3º (reading 480) rotor inflow angle. It is clear from its spectrum that the high A-weighted SPL and PNLT levels for the 3º (reading 480) rotor inflow angle are attributable to the 1F+1A tone for the forward emission angle. Note that this behavior is not observed at the aft emission angle, which shows increases of 0.9 and 3.5 dB as $\alpha_{Inflow}$ progresses from 0º (reading 470) to 3º (reading 480) to 8º (reading 488) for the 1F+1A tone.

The next most dominant tone is 1F+2A, which increases by 9.6 and 2.8 dB as $\alpha_{Inflow}$ progresses from 0º (reading 470) to 3º (reading 480) to 8º (reading 488) at the forward angle. At the aft angle, the level of this tone drops by 1.8 and 8.8 dB as $\alpha_{Inflow}$ progresses from 0º (reading 470) to 3º (reading 480) to 8º (reading 488). Levels of the other SO harmonics generally increase with increasing inflow angle for the aft emission angle.

The net effect is that the auralized flyovers sound more tonal at non-zero inflow angles than they do at the 0º inflow angle on the approach side. On the retreating side, the 0º and 3º auralizations sound similar, while the 8º is more dominated by the lower frequency 1F+1A tone. Auralizations of flyover noise associated with readings 480 and 488 are provided as supplemental audio.S9 and audio.S10, respectively. An interleaved version between the three conditions is provided in supplemental audio.S11.

### E. Effect of Ground Plane Reflections

As previously noted, the effect of a ground plane reflection produces a time-varying interference between the direct and ground reflected rays, which imparts a sound quality that is distinctive and familiar. Shown in Figure 23 are the A-weighed SPL and PNLT traces for an elevated receiver at 3.937 ft. (120 cm) above ground level for reading 361. In comparison to the relatively smooth traces for the flush receiver (see Figure 8 and Figure 9), these traces exhibit an irregular shape. The greater difference in EPNL (0.4 EPNdB) between the ANOPP and auralization methods indicated in Table 7 are largely attributable to differences in the irregularity of the PNLT traces, most of which occurs near the peak and on the retreating side.

Table 7: Effect of blade set (with and without ground plane interference) on EPNL.

| | | Flush Receiver | | Elevated Receiver | |
|---|---|---|---|---|---|
| Reading Number | Blade Set | ANOPP (EPNdB) | Auralization (EPNdB) | ANOPP (EPNdB) | Auralization (EPNdB) |
| 361 | F31/A31 | 111.3 | 111.3 | 108.5 | 108.1 |
| Gen-2 | Gen-2 | 100.5 | 100.2 | 97.6 | 97.5 |

A breakdown of tonal and broadband metrics is shown in Figure 24. Like the flush receiver breakdown shown in Figure 10, the approach side has a comparable contribution of tonal and broadband noise, while the retreating side is

dominated by the tonal component. Indeed, the greater irregularity observed in the tonal A-weighted SPL trace (compared with the relatively smooth broadband noise), in part, translates into greater irregularity in the associated PNLT trace. The greater irregularity in the tonal A-weighted SPL trace relative to the broadband trace been previously demonstrated to be due to differences in how the propagation is modeled.[10] Specifically, the auralization propagation is performed in the time domain and thus retains the phase relationship between direct and ground reflected rays, while that information is lost in the 1/3-octave band implementation within ANOPP. Broadband noise is less sensitive to this phenomenon because the phase distribution is random.

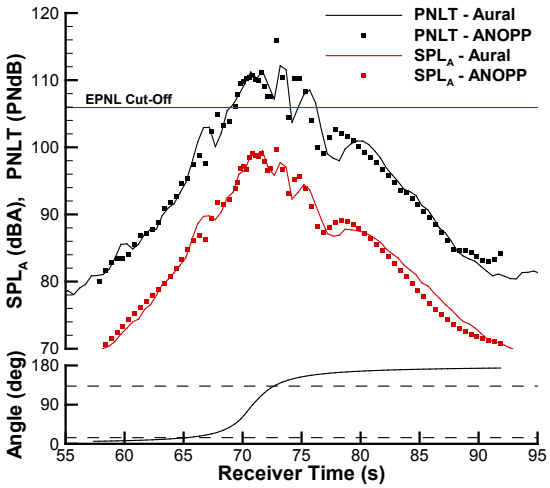


Figure 23: Effect of an elevated receiver on A-weighted SPL and PNLT for reading 361.

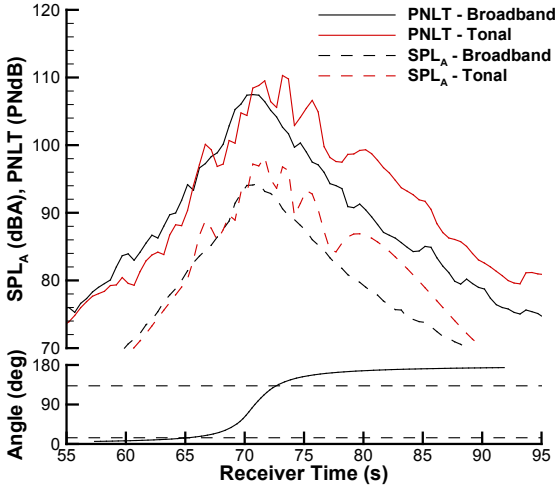


Figure 24: Breakdown of tonal and broadband metrics from auralization for reading 361 (elevated receiver).

Auralization of flyover noise for reading 361 with ground plane reflections is provided as supplemental audio.S12, with an interleaved version of the flush receiver provided in supplemental audio.S13. The interference effect is particularly pronounced at the overhead angles.

### F. Effect of Blade Set

The noise reduction associated with the Gen-2 blade set over the historical baseline is demonstrated for flush and elevated receivers for; a pylon-mounted installation, with pylon wake mitigation; zero rotor inflow angle; and comparable high thrust level. Due to the proprietary nature of the Gen-2 data, spectra, A-weighed SPL and PNLT plots are not presented. However, the noise reduction for the flush receiver is, on average, 11 EPNdB lower than the F31/A31 blade set, as indicated in Table 7. These results are consistent with previously published results generated independently by NASA[7,12] and GE.[5] It is noise reductions like this that have demonstrated that the Gen-2 design achieved aggressive noise goals, providing 15-17 EPNdB cumulative margin relative to Chapter 4 noise regulations.

For the flush receiver, the effect of the ground plane is a pressure doubling without interference effects. For the elevated receiver, interference between the direct and ground reflected rays is present, but the reduction of 10.8 EPNdB, averaged over ANOPP and auralization predictions, is comparable to the reduction found with the flush receiver. In other words, while the character of the sound is greatly affected by the interference due to ground plane reflections, that has negligible effect on the reduction of Gen-2 blade set noise relative to the historical blade set.

## Concluding Remarks

A method for auralizing flyover noise using model scale open rotor test data has been developed. It is based upon a process developed for system noise assessments,[12] but modified to allow noise to be synthesized independently for coherent tonal and incoherent broadband noise sources. This step is critical for generating open rotor source noise absent of undesirable artifacts. The synthesized source noise has been shown to have the same spectral characteristics as the narrowband data on which it is based. When propagated though an atmosphere to a ground receiver, the resulting noise metrics were shown to be in excellent agreement with those generated by the ANOPP system noise prediction tool. Differences in the metrics calculations in the presence of a ground plane are understood.

With this auralization capability, a number of investigations were conducted to understand the effects of thrust, installation type, rotor inflow angle, and the benefits of a second generation blade set. The effect of increased thrust was found to primarily affect the aft radiated 1F+2A combination tonal noise, leading to a higher EPNL. The pylon-mounted installation was found to incur a 1 EPNdB penalty over the isolated installation due to higher amplitude tones. Non-zero rotor inflow angle was found to increase tonal amplitudes and consequently EPNL by as much as 2 EPNdB. Finally, the second generation blade set was demonstrated to be substantially (11 EPNdB) quieter than the historical baseline blade set when running at comparable thrust levels. While these conclusions could as well be garnered from the system noise prediction, the true utility of the auralization is its ability to demonstrate noise benefits to stakeholders and practitioners alike, and to understand the psychoacoustic response associated with each configuration. With the gains made in open rotor noise reduction in recent years, perception-influenced designs are now possible which both meet noise certification requirements and simultaneously have desirable sound quality attributes.



## Acknowledgments

This work was performed with support from the Environmentally Responsible Aviation Project of the NASA Integrated Systems Research Program and the Fixed Wing and Aeronautical Sciences Projects of the NASA Fundamental Aeronautics Program. The GE Open Rotor blade design and testing were accomplished under the support of the FAA Continuous Lower Energy, Emissions and Noise Program.

## References

[1]Bowles, M.D., "The 'Apollo' of Aeronautics, NASA's Aircraft Energy Efficiency Program, 1973-1987," NASA SP-2009-574, January 2010.

[2]Janardan, B.A. and Gliebe, P.R., "Acoustic power level comparisons of model-scale counterrotating unducted fans," *29th Aerospace Sciences Meeting*, AIAA-91-0595, Reno, NV, 1991.

[3]Hoff, G.E., "Experimental performance and acoustic investigation of modern, counterrotating blade concepts," NASA CR-185158, January 1990.

[4]Harris, R.W. and Cuthbertson, R.D., "UDF™/727 Flight Test Program," *AIAA/SAE/ASME/ASEE 23rd Joint Propulsion Conference*, AIAA-87-1733, San Diego, CA, 1987.

[5]Khalid, S.A., et al., "Open rotor designs for low noise and high efficiency," *Proceedings of the ASME Turbo Expo 2013*, GT2013-94736, San Antonio, TX, 2013.

[6]Van Zante, D.E., Collier, F., Orton, A., Khalid, S.A., Wojno, J.P., and Wood, T.H., "Progress in open rotor propulsors: The FAA/GE/NASA open rotor test campaign," *To appear in the Aeronautical Journal*, Royal Aeronautical Society, 2014.

[7]Hendricks, E.S., Berton, J.J., Haller, W.J., Tong, M.T., and Guynn, M.D., "Updated assessments of an open rotor airplane using advanced blade designs," *49th AIAA/ASME/SAE/ASEE Joint Propulsion Conference*, AIAA-2013-3628, San Jose, CA, 2013.

[8]Rizzi, S.A., Sullivan, B.M., and Aumann, A.R., "Recent developments in aircraft flyover noise simulation at NASA Langley Research Center," *NATO Research and Technology Agency AVT-158 "Environmental Noise Issues Associated with Gas Turbine Powered Military Vehicles" Specialists' Meeting*, Paper 17, Montreal, Canada, 2008, NATO RTA Applied Vehicle Technology Panelpp. 14.

[9]Zorumski, W.E., "Aircraft noise prediction program theoretical manual," NASA TM-83199, 1982.

[10]Rizzi, S.A., Aumann, A.R., Lopes, L.V., and Burley, C.L., "Auralization of hybrid wing body aircraft flyover noise from system noise predictions," *51st AIAA Aerospace Sciences Meeting*, AIAA-2013-0542, Grapevine, TX, 2013.

[11]Envia, E., "Open rotor aeroacoustic modelling," *Conference on Modelling Fluid Flow (CMFF'12), The 15th International Conference on Fluid Flow Technologies*, Budapest, Hungary, 2012.

[12]Guynn, M.D., Berton, J.J., Haller, W.J., Hendricks, E.S., and Tong, M.T., "Performance and environmental assessment of an advanced aircraft with open rotor propulsion," NASA TM-2012-217772, October 2012.

[13]Wojno, J.P. and Janardan, B.A., "Comparison of NASA 9x15 low speed wind tunnel counter rotating open rotor data with GE-anechoic facility historic data for baseline F31A31 blade design," *19th AIAA/CEAS Aeroacoustics Conference*, AIAA 2013-2204, Berlin, Germany, 2013.

[14]Van Zante, D.E., Gazzaniga, J., Elliott, D.M., and Woodward, R., "An open rotor test case: F31/A31 historical baseline blade set," *20th ISABE Conference*, ISABE-2011-1310, Gothenburg, Sweden, 2011.

[15]Elliott, D.M., "Initial investigation of the acoustics of a counter rotating open rotor model with historical baseline blades in a low speed wind tunnel," *17th AIAA/CEAS Aeroacoustics Conference*, AIAA 2011-2760, Portland, Oregon, 2011.

[16]"Octave, half-octave, third octave band filters intended for the analysis of sounds and vibrations," International Electrotechnical Commission (IEC) Publication 225, 1966.

[17]Parry, A.B., Kingan, M., and Tester, B.J., "Relative importance of open rotor tone and broadband noise sources," *17th AIAA/CEAS Aeroacoustics Conference*, AIAA-2011-2763, Portland, OR, 2011.

[18]Rizzi, S.A. and Sullivan, B.M., "Synthesis of virtual environments for aircraft community noise impact studies," *11th AIAA/CEAS Aeroacoustics Conference*, AIAA-2005-2983, Monterey, CA, 2005.

[19]Rizzi, S.A., Aumann, A.R., Allen, M.P., Burdisso, R., and Faller II, K.J., "Simulation of rotary and fixed wing flyover noise for subjective assessments (Invited)," *161st Meeting of the Acoustical Society of America*, Seattle, WA, 2011.
[20]Allen, M.P., Rizzi, S.A., Burdisso, R., and Okcu, S., "Analysis and synthesis of tonal aircraft noise sources," *18th AIAA/CEAS Aeroacoustics Conference*, AIAA-2012-2078, Colorado Springs, CO, 2012.
[21]Okcu, S., Allen, M.P., and Rizzi, S.A., "Psychoacoustic assessment of a new aircraft engine fan noise synthesis method," *164th Meeting of the Acoustical Society of America*, Kansas City, MO, 2012.
[22]Grosveld, F.W., Sullivan, B.M., and Rizzi, S.A., "Temporal characterization of aircraft noise sources," *42nd AIAA Aerospace Sciences Meeting*, AIAA-2004-1029, Reno, NV, 2004.
[23]Laakso, T.I., Välimäki, V., Karjalainen, M., and Laine, U.K., "Splitting the Unit Delay -Tools for Fractional Delay Filter Design," *IEEE Signal Processing Magazine*, Vol. 13, No. 1996, pp. 30-60.
[24]"GoldServe, AuSIM3D Gold Series Audio Localizing Server System, User's Guide and Reference, Rev. 1d," AuSIM Inc. Mountain View, CA, October 2001.
[25]Arntzen, M., Rizzi, S.A., Visser, H.G., and Simons, D.G., "A framework for simulation of aircraft flyover noise through a non-standard atmosphere," *18th AIAA/CEAS Aeroacoustics Conference*, AIAA 2012-2079, Colorado Springs, CO, 2012.
[26]Delany, M.E. and Bazley, E.N., "Acoustical properties of fibrous absorbent materials," *Applied Acoustics*, Vol. 3, No. 2, 1970, pp. 105-116.
[27]Zölzer, U., ed. DAFX - Digital audio effects. John Wiley & Sons, Ltd., West Sussex, England, 2002.
[28]Lopes, L.V. and Burley, C.L., "Design of the next generation aircraft noise prediction program: ANOPP2," *17th AIAA/CEAS Aeroacoustics Conference*, AIAA 2011-2854, Portland, Oregon, 2011.
[29]"Aircraft flyover simulation," http://stabserv.larc.nasa.gov/flyover/, NASA, 2014.
[30]Brandvik, T., Hall, C., and Parry, A.B., "Angle-of-attack effects on counter-rotating propellers at take-off," *Proceedings of the ASME Turbo Expo 2012*, GT2012-69901, Copenhagen, Denmark, 2012.